

**Chemical Vapor Deposition of Carbon Nanostructures and
Carbon Nanotubes-Reinforced Composites**

by

Chi-Hwa Wu

Submitted in Partial Fulfillment

of the

Requirements for the Degree

Doctor of Philosophy

Supervised by

Professor David R. Harding

Department of Chemical Engineering
The College
School of Engineering and Applied Sciences

University of Rochester
Rochester, New York

2006

CURRICULUM VITAE

The author was born in Taipei, Taiwan on June 14, 1976. He attended Tunghai University from 1994 to 1998, and graduated with a Bachelor of Science degree in 1998. He came to the University of Rochester in the Fall of 2000 and began graduate studies in Chemical Engineering. He received a Frank J. Horton Research Fellowship from 2001 to 2006. He pursued his research in polymeric composite materials with nanostructures reinforcement under the direction of Professor David R. Harding and received the Master of Science degree from the University of Rochester in 2004.

ACKNOWLEDGEMENTS

I would like to thank my research advisor Professor David R. Harding for his support and guidance. This dissertation would not have been possible without his encouragement and help throughout my years of graduate study. I thank Messrs. M. Bonino, D. Turner, M. Wittman, S. Noyes, R. Gram, D. Guy, S. Scarantino, R. Janezic, K. Lintz, , J. Sailer, and L. Elasky of the Target Fabrication Group at Laboratory for Laser Energetics for technical assistance and support, Mr. B. McIntyre of the Institute of Optics of University of Rochester for assistance with electron microscopy, and Mrs. C. Pratt of the Department of Mechanical Engineering of University of Rochester for assistance with nano-indentation. I thank my fellow students A. Knight and M. Bobeica for their helpful discussions and help. I also thank Dr. F.Y. Tsai, a former member of the Target Group, for his encouragement and support throughout my Ph.D. study, and with whom I have been lucky enough to maintain a closed and cherished friendship.

I appreciate the support in the form of a Frank J. Horton Research Fellowship from the Laboratory for Laser Energetics. This work was supported by the U.S. Department of Energy Office of Inertial Confinement Fusion under Cooperative Agreement No. DE-FC52-92SF19460, the University of Rochester, and the New York State Energy Research and Development Authority. The support of DOE does not constitute an endorsement by DOE of the views expressed in this article.

I would also like to especially thank my parents K.T. and Lu-Chu, my sisters Emily and Jenny, and my girlfriend, Y. Yang, for their unconditional love and encouragement as I pursued this goal.

ABSTRACT

The vapor deposition of open-networked carbon nanostructures and carbon nanotubes (CNTs)-reinforced composites have been developed and studied parametrically. Carbon nanostructures, including nano-tubes, nano-foams, nano-particles, and nano-walls, have been deposited on catalyst-assisted substrates using microwave plasma electron cyclotron resonance-chemical vapor deposition (ECR-CVD) system at temperature as low as 300 °C. Processing parameters determining the morphologies and properties of the nanostructures were identified to optimize the productions.

Carbon nanotubes-reinforced polymer composite films were synthesized at low temperature by a two-step process using: (1) ECR-CVD system to vapor deposit a nanotube film substrate at 480 °C with gas mixture of methane and hydrogen, and (2) chemical vapor infiltration (CVI) of hydrocarbon (CH) polymers into the nanotube substrate. In this study, parylene and glow-discharge polymerization (GDP) polymers were utilized to infiltrate the nanotube substrate at temperature below 70 °C. A strong interfacial adhesion between the carbon nanotubes and the polymer matrix is a major factor that determines the reinforcement performance of such nanocomposites. Scanning electron microscopy (SEM) and transmission electron microscopy (TEM) studies showed that nanotubes embedded within the

polymer matrix not only provide a chemically compatible interface with the polymer but also enhance interfacial adhesion by mechanical interlocking or entangling.

The feasibility of making carbon nanotubes-reinforced composite depends on the processing parameters, including the effect of polymer vapor infiltration and the volume density of the nanotube substrate. Characterizations of these composite films have been conducted and it was found that vapor-deposited parylene/CNTs composite possessed better interfacial bonding and an infiltration distance ~200% greater than the GDP/CNTs one, while using a 39 vol.% nanotube substrate. In addition, analyses via nano-indentation measurement revealed that the effect of nanotubes reinforcement within the composite resulted in 14% increase in elastic modulus.

TABLE OF CONTENTS

Chapter 1. Introduction	1
1.1 Carbon Nanotubes	1
1.2 Structures and Properties of Carbon Nanotubes	3
1.3 Carbon Nanotubes-Reinforced Polymer Composites for Use as ICF Targets	5
1.3.1 Inertial Confinement Fusion	5
1.3.2 Target Requirements	6
1.3.3 Carbon Nanotubes-Reinforced Polymer Microcapsules	7
1.4 Objective	8
1.5 Figures and Tables	11
Chapter 2. Fabrication of Carbon Nanotubes by Microwave Plasma Chemical Vapor Deposition	19
2.1 Introduction	19
2.1.1 Synthesis Methods of Carbon Nanotubes	19
2.1.2 Growth Mechanism of Carbon Nanotubes	22
2.2 Experimental	23
2.2.1 Materials	23
2.2.2 Procedures and Apparatus	24
2.2.3 Characterization	26
2.3 Deposition of Carbon Nanotubes	27
2.3.1 Morphology of Carbon Nanotubes	27
2.3.2 Growth Rate of Carbon Nanotubes	30
2.4 Effects of Processing Conditions	31

2.4.1 Electron Cyclotron Resonance	31
2.4.2 Deposition Pressure and CH ₄ Concentration	32
2.4.3 Substrate Temperature	34
2.4.4 Substrate Bias	35
2.5 Properties of Vapor-Deposited Carbon Nanotubes Films	36
2.6 Summary	37
2.7 Tables and Figures	39
Chapter 3. Vapor Deposition of Open-Networked Carbon Nanostructures at Low Temperature	62
3.1 Introduction	62
3.2 Experimental	63
3.2.1 Catalysts Preparation	63
3.2.2 Procedures and Characterizations	64
3.3 Results and Discussion	66
3.3.1 Morphology of Vapor-Deposited Carbon Nanostructures	66
3.3.1.1 Carbon Nano-Foams	66
3.3.1.2 Carbon Nano-Particles	68
3.3.1.3 Carbon Nano-Walls	69
3.3.2 Effects of Processing Conditions	71
3.3.2.1 Catalyst-Assisted Substrates	71
3.3.2.2 Substrate Temperature	73
3.3.2.3 Substrate Bias	74
3.4 Properties of Vapor-Deposited Carbon Nanostructures	74
3.5 Summary	75
3.6 Tables and Figures	77

Chapter 4. Chemical Vapor Deposition of Carbon Nanotubes-Reinforced Polymer Composites	96
4.1 Introduction	96
4.1.1 Background: CNTs Properties Critical to Reinforcing Composites	96
4.1.2 Growth of Carbon Nanotubes-Reinforced Composites	100
4.2 Vapor Deposition of Polymer	102
4.2.1 Glow Discharge Polymerization	103
4.2.2 Parylene Coating Process	104
4.3 Experimental	105
4.3.1 MWNTs Thin Film Substrates	106
4.3.2 Vapor Deposition and Infiltration of Polymers	106
4.3.3 Characterizations	110
4.4 Results and Discussion	111
4.4.1 Processing of Vapor-Deposited Composites	111
4.4.1.1 Deposition Rate of Polymer	111
4.4.1.2 Low Temperature Deposition	113
4.4.2 Nanotubes-Reinforced Polymer Composites	114
4.4.2.1 Interfacial Characterizations	114
4.4.2.2 Nanotubes Reinforcement	118
4.4.3 Properties of Carbon Nanotubes-Reinforced Composites	119
4.5 Summary	121
4.6 Tables and Figures	123
Chapter 5. Summary	152
References	157
Appendix A. Derivation of the Proposed Equations for the MWNTs system	167

LIST OF TABLES

Table 1.1 Mechanical properties of CNTs compared with other materials [2,4-6,16,17]	11
Table 1.2 Mechanical performance of the multi-walled carbon nanotubes (MWNTs) and vapor-grown carbon fibers (VGCF) as reinforcements for polystyrene (PS) composites [19]	12
Table 1.3 Designs of Inertial Confinement Fusion (ICF) targets for various laser facilities [21,22]	13
Table 2.1 Common methods of carbon nanotubes productions	39
Table 2.2 Typical processing conditions of H ₂ plasma pretreatment for the catalyst-assisted substrates	40
Table 2.3 Summary of the processing conditions for the CNTs production using ECR-CVD system	41
Table 2.4 Measurements of diameters of the typically as-deposited MWNTs	42
Table 2.5 Effects of the ECR microwave power on the morphologies of vapor-deposited carbon nanotubes	43
Table 2.6 Properties of vapor-deposited MWNTs films by ECR-CVD compared with those of MWNTs produced by other methods. Include the properties of individual MWNTs as reference	44
Table 3.1 Processing conditions for the deposition of carbon nanostructures by ECR-CVD system	77
Table 3.2 Processing conditions for the deposition of carbon nano-foams	78
Table 3.3 Processing conditions for the deposition of carbon nano-particles	79
Table 3.4 Effects of the processing conditions on the morphologies of vapor-deposited carbon nanostructures	80
Table 3.5 Properties of vapor-deposited carbon nano-walls by ECR-CVD compared with those of MWNTs film	81
Table 4.1 Summary of the processing conditions for the GDP production	123
Table 4.2 Summary of the processing conditions for the parylene coating system	124
Table 4.3 Average coating rate of the GDP deposition subjected to 20 and 40W RF plasma power under various coating time. All samples were located at the center of the coating chamber (18.5 cm away from the resonator)	125
Table 4.4 Summary of the GDP infiltration distances at different substrate locations under 40W RF power for 25 hours deposition	126

Table 4.5	Effect of the RF power and coating time on the infiltration distance of the GDP within the MWNTs substrate	127
Table 4.6	Effect of using GDP and parylene coating processes on the infiltration distance of polymer within the CNTs over various coating time	128
Table 4.7	Properties of vapor-deposited parylene/CNTs composites compared with those of 39 and 71 vol. % MWNTs films	129

LIST OF FIGURES

Figure 1.1	(a) A graphene sheet made of carbon atoms placed at the corners of hexagons forming the lattice with chiral vector, $\mathbf{Ch} = n\mathbf{a}_1 + m\mathbf{a}_2$ (\mathbf{a}_1 and \mathbf{a}_2 are the unit vectors) denoting the rolling direction of the sheet to make (b) a (5,5) armchair nanotube, a (9,0) zigzag nanotube, and a (10, 5) chiral nanotube [14]	14
Figure 1.2	TEM images of typical (a) SWNTs, and (b) MWNTs [1,14]	15
Figure 1.3	Schematic of the carbon nanotubes-based field effect transistor [9,10]	16
Figure 1.4	Schematics of the Inertial Confinement Fusion (ICF) process [20]	17
Figure 1.5	Schematics of the typical targets with (a) nanotubes-reinforced shell walls and (b) nanotubes-reinforced DT layers inside the walls	18
Figure 2.1	Growth mechanism of carbon nanotubes on metal (M) catalyst -assisted substrate by chemical vapor deposition. CH_4 was used as the carbon source [44,45]	45
Figure 2.2	Schematic of the fabrication process of catalyst-assisted substrates	46
Figure 2.3	Setup of the electron cyclotron resonance- chemical vapor deposition (ECR-CVD) system	47
Figure 2.4	SEM images of as-deposited MWNTs, (a) side-view and (b) top-view. Growth conditions (bias voltage=-200V, CH_4 : H_2 = 7.5:30, substrate temperature =480°C) were used for the deposition	48
Figure 2.5	SEM images of MWNTs, (a) grown on cobalt-assisted substrates, and (b) obvious catalyst particles at the tip of tubes. Growth conditions were the same as those in Fig. 2.4	49
Figure 2.6	TEM micrograph of a catalyst particle fully enclosed within one end of the MWNT	50
Figure 2.7	Cross-sectional SEM images of (a) a multi-walled nanotube shown hollow structure, and (b) measurement of inner and outer diameters of the tube	51
Figure 2.8	Schematic of a multi-walled nanotube with average density of 1.86 g/cm^3 calculated from Equation (2-1) and (2-2)	52
Figure 2.9	Calculated density of MWNTs as a function of the ratio of inner and outer tube diameters. As the ratio increases (fewer layers in a tube), the density is closed to the single-walled nanotube of 1.33 g/cm^3	53
Figure 2.10	Average MWNTs length as a function of growth time. Note that the diameters of nanotubes remained at $\sim 50 - 80 \text{ nm}$ even as the growth time increased	54

Figure 2.11	SEM images of MWNTs grown with microwave powers of (a) 200W, (b) 500W, and (c) 600W	55
Figure 2.12	SEM images of MWNTs grown at pressures of (a) 7 mTorr, (b) 14.1 mTorr, and (c) 19.6 mTorr	56
Figure 2.13	MWNTs length and diameter as a function of growth pressure	57
Figure 2.14	Average MWNTs length and diameter as a function of CH ₄ concentration	58
Figure 2.15	SEM images of MWNTs grown with substrate temperatures of (a) 150 °C, (b) 300 °C, and (c) 480 °C	59
Figure 2.16	Average MWNTs length and diameter as a function of substrate bias	60
Figure 2.17	Typical modulus-displacement data acquired by nano-indentation with a carbon nanotube film sample	61
Figure 3.1	Setup of the sputtering coater for the Ni catalyst deposition. The processing time is 3 min	82
Figure 3.2	SEM images of (a) open-networked carbon nano-foams, and (b) a magnified image of the foams with various pore sizes	83
Figure 3.3	SEM images of nano-foams grown at 400 °C with (a) denser networks than those at 300°C, and (b) more uniform and well-distributed pore sizes	84
Figure 3.4	SEM images of (a) aligned and vertical nano-foams grown with -50V substrate bias, and (b) randomly distributed nano-foams without bias application	85
Figure 3.5	SEM images of (a) the typical surface of a nano-particles film, and (b) nano-particles with average diameters in a range of 20 -100 nm	86
Figure 3.6	SEM images of nano-particles grown for 60 min with (a) uniform and continuous surfaces, and (b) ~100% increase in diameters compared with those of 15 min deposition	87
Figure 3.7	SEM images of nano-particles grown at -50V bias with (a) a wavy surface, and (b) the same particle sizes as those grown at -100V	88
Figure 3.8	SEM images of typical carbon nano-walls by ECR-CVD, (a) two-dimensional wall-like structures, and (b) vertically aligned carbon nano-walls	89
Figure 3.9	SEM images of (a) a close-up carbon nano-walls showing vertical alignment, and (b) the measurement of carbon nano-walls. The wall thickness and height were approx. 20-100, 500 nm, respectively	90
Figure 3.10	SEM images of the nano-walls at different growth stages, (a) after a growth of 3 min, (b) after 5 min, and (c) after 15 min	91
Figure 3.11	Average wall height and thickness of nano-walls as a function of growth time	92

Figure 3.12	The surface morphologies of catalyst-coated substrates after H ₂ plasma pretreatment for 10 min, respectively, of (a) spherical Co particles, and (b) T-shape Fe particles	93
Figure 3.13	The wall thickness of carbon nano-walls and the diameter of nano-particles, respectively, as a function of substrate bias	94
Figure 3.14	Typical modulus-displacement data acquired by nano-indentation of carbon nano-walls film deposited by ECR-CVD	95
Figure 4.1	Stresses acting on a segment of nanotube in a composite [86,87]	130
Figure 4.2	Effect of the nanotube diameter, D_{CNT} , and critical length, l_c , on the nanotube-polymer interfacial shear strength, τ_{CNT} [88,89]	131
Figure 4.3	Schematic of fabrication procedures for the nanotubes/polymer composites using chemical vapor deposition (CVD) and vapor infiltration (CVI) techniques	132
Figure 4.4	Procedures of vapor depositing a uniform layer of GDP thin film on top of the nanotube substrate	133
Figure 4.5	General structure of (a) parylene N, (b) parylene C, and (c) parylene D	134
Figure 4.6	Typical synthesis scheme of parylene	135
Figure 4.7	Schematics of a two-step procedure for the CNTs-reinforced composites	136
Figure 4.8	Setup of the glow discharge polymerization (GDP) deposition system	137
Figure 4.9	Setup of the parylene coating system	138
Figure 4.10	GDP coating rate as a function of substrate position	139
Figure 4.11	SEM images of (a) 50 hr GDP deposition with a MWNTs substrate, and (b) a fracture surface of GDP/CNTs interface	140
Figure 4.12	SEM images of (a) the typical interface of a nanotubes-reinforced GDP composite, and (b) an enlarged images of the GDP/CNTs interface	141
Figure 4.13	SEM images of GDP/CNTs composites grown with 20W RF power, (a) exhibition of partial densification of polymer, and (b) a magnified image of the interface showing nanotubes embedded within the GDP polymer	142
Figure 4.14	Top-viewed SEM images of GDP/CNTs composite grown for (a) 5 hrs, (b) 25 hrs, and (c) 250 hrs	143
Figure 4.15	SEM images of a typical parylene/CNTs composite	144
Figure 4.16	SEM images of (a) typical interface between parylene polymer and CNTs, and (b) a magnified morphology showing the contact and adherence of the polymer to most of the nanotubes	145

LIST OF SYMBOLS AND ABBREVIATIONS

SYMBOLS

\mathbf{a}_1	unit vector of the hexagonal lattice (dimensionless)
\mathbf{a}_2	unit vector of the hexagonal lattice (dimensionless)
\mathbf{C}_h	chiral vectors in the graphene plane (dimensionless)
D_{CNT}	outer diameter of carbon nanotube (L)
d_{CNT}	inner diameter of carbon nanotube (L)
L_c	critical length of carbon nanotubes (L)
n_{PA}	refractive index of parylene (dimensionless)
t_{PA}	parylene thickness per fringe (L)
vol_{inner}	volume of inner (hollow) tube (L^3)
vol_{outer}	volume of outer (tubular) tube (L^3)
$\rho_{graphite}$	density of graphite (ML^{-3})
ρ_{CNT}	density of individual multi-walled carbon nanotube (ML^{-3})
σ_{CNT}	tensile strength of a nanotube segment ($ML^{-1}t^{-2}$)
τ_{CNT}	nanotube-polymer interfacial shear strength ($ML^{-1}t^{-2}$)
λ	IR laser wavelength (L)

ABBREVIATIONS

AFM	atomic force microscope
CH	hydrocarbon
CNTs	carbon nanotubes
CSM	continuous stiffness measurement
CVI	chemical vapor infiltration

CVD	chemical vapor deposition
ECR-CVD	electron cyclotron resonance chemical vapor deposition
FEDs	field emission displays
GDP	glow discharge polymerization
ICF	inertial confinement fusion
LLE	Laboratory for Laser Energetics
MWNTs	multi-walled carbon nanotubes
NIF	National Ignition Facility
PAMS	poly- α -methylstyrene
PHAE	polyhydroxyaminoether
PMMA	polymethylmethacrylate
PS	polystyrene
SEM	scanning electron microscopy
SWNTs	single-walled carbon nanotubes
TEM	transmission electron microscopy
VDP	vapor deposition polymerization
VGCF	vapor grow carbon fiber

Chapter 1. Introduction

1.1 Carbon Nanotubes

Since discovered in 1991 [1] as elongated fullerenes, carbon nanotubes (CNTs) have introduced an important opportunity to the fields of scientific and engineering worlds with their superior properties and outstanding geometrical dimensions. Carbon nanotubes can be described as a hexagonal sheet of carbon atoms rolled into a seamless cylindrical shape, as shown in Figure 1.1. A nanotube is composed entirely of sp^2 bonds structure, which is similar to those of graphite and provides the molecules with its unique strength. A typical nanotube has outer diameters varying between 1-2 and few tens of nanometers when it was first discovered, while the inner hollow diameter is typically of the order of only 1 to 5 nm [2,3]. There are two types of nanotubes: single-walled nanotubes (SWNTs) and multi-walled nanotubes (MWNTs), as shown in Figure 1.2 (a) and (b), respectively. The detailed structures and properties will be described in the next section.

Besides their extremely small size, it has been suggested that carbon nanotubes possess tensile strengths at least 100 times stronger than high strength steel alloys [4], have current capacities 1000 times higher than copper [4,5], and transmit heat twice as well as pure diamond [6]. To take advantage of this unique combination of

size and properties, researchers have been exploring the potential of CNTs in a wide variety of applications. For example, CNTs have been experimentally demonstrated as an atomic force microscope (AFM) tip for imaging and lithography [7,8]. With extremely small sizes and good conductivity of CNTs, this tip now can be made as small as few nm offering reasonable resolution. In addition, the remarkable electronic properties of nanotubes enable them for use as quantum wires to bridge a junction device, as shown in Figure 1.3, for the nanoelectronics applications [9,10]. Also, the geometric properties of CNTs, such as the high aspect ratio, mechanical strength and chemical stability, qualify them an ideal candidate for the electron field emission displays (FEDs) [11-13]. Other than these thermal and electrical applications, second major application will be based on nanotube strength, elasticity and mechanical properties including mechanical memory, supersensitive sensors, hydrogen and ion storages, and nano-structural materials. While the outstanding properties of carbon nanotubes have led to a wide range of applications, in this study here we limit our analysis to the use of carbon nanotubes as a filler for structural reinforcement in a host polymer matrix, a material referred to as a *carbon nanotube-reinforced polymer composites*, which is one of the main subject of this study and will be discussed in detail in Chapter 4.

1.2 Structures and Properties of Carbon Nanotubes

Carbon nanotubes are fullerene-related structures, which is aforementioned as a piece of graphene sheet to form a cylinder with end caps containing pentagonal rings. The role of a pentagonal ring defect is to produce a convex structure, which helps to form the curved structures and close the tube at two ends [14]. In the mapping of a graphene plane into a cylinder, chiral vector $C_h = n a_1 + m a_2$ is defined in terms of the lattice translation indices (n, m) and the unit vectors a_1 and a_2 of the hexagonal lattice, as shown in Figure 1.1(a), to identify and determine the directions along which the graphene sheets are rolled to form tubular structures. The nanotubes of type (n, n) in Figure 1-1(b) are commonly called armchair nanotubes with a symmetry $\backslash _ / _ /$ shape. Another type of nanotubes $(n, 0)$ is known as zigzag nanotubes because of the $\backslash _ _ /$ shape along the axis. All other types of nanotubes could be defined as a pair of indices (n, m) , where $n \neq m$ [14]. The electronic conductivity of nanotube is highly sensitive to a change of these parameters, which determines a carbon nanotube being either metallic or semiconducting [14,15].

Interest in nanotubes for nano-scale material applications exists due to a number of extraordinary properties:

- (1) Single and multi-walled carbon nanotubes have very good mechanical properties. The tensile modulus and strength of the nanotubes ranging

from about 270 GPa to 1 TPa and 11-200 GPa, respectively, have been reported [16, 17], making nanotubes perhaps the ultimate high stiffness reinforcement material. Table 1.1 shows the mechanical properties of CNTs with other materials [2,4-6,16,17]. It indicates that CNTs possess most superior mechanical characteristic.

- (2) Nanotubes possess hollow and closed topology that produce a distinct mechanical response compared to other graphitic structures. Nanotubes can sustain extreme strains (40%) in tension without showing signs of brittle, behavior, plastic deformation, or bond rupture [18].
- (3) Nanotubes are lightweight, high aspect-ratio structures and could be the ideal packing materials for gas-storage and hydrocarbon fuel storage devices [14].

It is also worth noting that the carbon nanotubes are chemically and molecularly defined structures with reproducible dimensions that make them stiffer and stronger than any potentially known material with applications for the design of polymer composites. Early evaluations of carbon nanotubes indicated they possess outstanding mechanical properties – greater than those of vapor grow carbon fiber (VGCF), a reinforcement fiber usually employed in materials and aerospace applications. Table 1.2 lists an example of CNTs and VGCF as reinforcement within a polystyrene (PS) polymer matrix [19]. The higher elastic modulus of nanotubes with a tensile strength an order of magnitude higher than that of

conventional carbon fibers qualifies the nanotubes as a desirable reinforcement in polymer composite materials.

1.3 Carbon Nanotubes-Reinforced Polymer Composites for Use as ICF Targets

1.3.1 Inertial Confinement Fusion

The main mission of the Laboratory of Laser Energetics (LLE) at the University of Rochester is to investigate inertial confinement fusion (ICF) using the direct-drive approach. Inertial confinement fusion is a process where the fuel is confined by its own inertia for a sufficiently long time at very high density and temperature for the fusion reaction to occur. This is achieved by uniformly illuminating a target that consists of a thin-wall shell with a concentric solid fuel (DT or D₂) with the sixty beams of the 30 kJ Omega laser thereby compressing its contents to a density and pressure sufficient to initiate nuclear fusion. The laser beams instantaneously ionize the atoms in the outermost layer of the target and heat the resultant plasma. As the plasma ablates and expands outwards, the remainder of the fuel accelerates inwards, compressing the central region until the fuel is 1000 liquid density, which

raises the fuel temperature to trigger the fusion reaction [20]. The schematic of direct-drive ICF process is shown in Figure 1.4.

1.3.2 Target Requirements

A spherical target typically consists of a thin-wall polymer capsule that is ~ 1 mm in diameter with a wall thickness of 3-5 μm and a uniform solid fuel (DT or D_2) layer (100 μm thick) on its inner surface. Foam shells having densities of 70 - 120 mg/cc and thickness of 40 – 60 μm will be coated with a normal density plastic layer. The preparation of these targets will be greatly facilitated if the capsule possesses the following properties: (i) high gas permeability at elevated temperature to allow a rapid fill with DT; (ii) high strength and elastic modulus to withstand greater buckling/bursting pressures and thus be filled more rapidly than current targets; (iii) good thermal conductivity that may help the layering process by creating a more isothermal environment for the ice; (iv) substantial transparency in the visible spectrum to allow observation during DT filling.

The design of the ICF target varies with the different laser facilities employed to conduct the experiment. Table 1.3 lists the target designs for the main current laser facilities [21, 22]. It is noted that direct-drive ICF experiments on the National Ignition Facility (NIF), whose energy is almost 50 times larger than OMEGA's energy, require targets with larger diameters (3.5mm) and comparable thick wall

for OMEGA targets (3 μm); achieving the surface smoothness, uniform wall thickness, and sphericity of these targets is considerable more difficult as the target size increases.

1.3.3 Carbon Nanotubes-Reinforced Polymer Microcapsules

Various materials have been used to fabricate shells for use as ICF fuel capsules [21]. Previous and current processes for the production of ICF targets have been dedicated to developing plastic shells for their mechanical properties, high permeability, optical transparency and low atomic number and low density. Those plastic materials that are available for use in the OMEGA application include polystyrene (PS) [23], poly- α -methylstyrene (PAMS) [24], vapor deposition polymerization (VDP) polyimide [25], and hydrocarbons capsules fabricated using a glow-discharge-polymerization (GDP) process [26]. Such materials with promising properties have been greatly beneficial in target fabrication. The next generation of shells for the NIF or Fusion energy will have to be permeation-filled more rapidly with the DT fuel, because the larger size has a comparably larger fuel inventory. Therefore, the possibility of making a strong plastic shell by reinforcing it with carbon nanotubes (CNTs) reinforcement is investigated to meet this challenge.

Carbon nanotubes could benefit target fabrication in the following two ways: First, due to the greater strength and toughness of the reinforcing CNTs and interfacial bonding for load transfer, “whisker-like” carbon nanotubes reinforcing the plastic shell wall, as shown in Figure 1.5 (a), can make the shell withstand greater buckling/bursting pressures and thus be filled more rapidly than current targets. The carbon content of nanotube reinforcement could also provide increased laser absorption with which the lower density would minimize the hydrodynamic penalty. Moreover, carbon nanotubes also possess high thermal conductivity that may help the layering process by creating a more isothermal environment for the ice. Second, carbon nanotubes can function like foams, inside a shell as shown in Figure 1.5 (b), to support DT ice and help creating an ideal structure for the target. The open connectivity of the CNTs-type foam would benefit the ice layering process by providing a more “open” and connective radial path through the foam wall.

1.4 Objective

Carbon nanotubes (CNTs) have been recognized as ideal reinforcement materials in other technology fields [7-14]. A great deal of recent research has focused on limiting the defects within the nanotubes (which are particularly detrimental from a mechanical property perspective) and increasing the production yields from

nanotube processing techniques. Current nanotubes-reinforced nanocomposites are usually prepared by “wet” processing methods, such as solution mixing and casting, melt dispersion, or extrusion and injection techniques. Those techniques; however, have few limitations and do not achieve expected properties due to, (i) poor separation of bundles: there are types of nanotubes that are produced as bundles. In order to have an optimal load transfer from the matrix to the nanotubes, they must be separated; (ii) weak nanotube-polymer interface: these wet processing methods do not yield a homogeneous and stable interface between nanotube and polymer matrix. Also, at the moment the efforts to make CNTs or nanotube-reinforced composites at low temperature needed for ICF application have failed to achieve properties equivalent to those of high-temperature productions.

Therefore, the attraction of this study is the potential to determine the feasibility of making carbon nanotubes-reinforced polymer composite thin films or shells with desirable low temperature and great mechanical properties for target fabrication, and using only chemical vapor deposition (CVD) and vapor deposited polymerization processes.

The main goals are:

- (1) Develop a fabrication process for production of vapor-deposited carbon nanotubes at low temperature with desirable mechanical properties and dimensions for ICF application.

- (2) Optimize the vapor deposition with different processing conditions to produce other types of low temperature open-networked carbon nanostructures, including nano-foams and nano-walls.
- (3) Develop a series of fabrication procedure to synthesize carbon nanotubes-reinforced polymer composites using only vapor deposition process.
- (4) Identifying and characterizing the interfacial interaction between nanotubes and polymer matrix.
- (5) Characterize the composites quality and properties relevant to the ICF applications, including tensile strength, mechanical modulus, composite densities, and shell wall thickness uniformity.

1.5 Tables and Figures

Materials	Diameter (nm)	Density (g/cm³)	Modulus (GPa)	Tensile Strength (GPa)
CNTs	1-10	1.33-2.6	Up to ~1000	Up to ~200
C Nanoropes	10-100	1.3	563	~75
SiC fibers	10,000- 20,000	2.3	190	2.8
Quartz	9,000	2.2	70	3.4
Steel	-	7.8	208	0.4
Epoxy	-	1.25	3.5	0.05
Wood	-	0.6	16	0.08

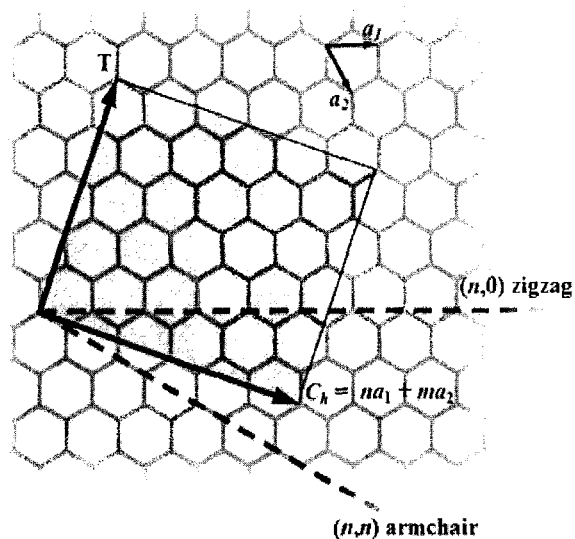
Table 1.1 Mechanical properties of CNTs compared with other materials [2,4-6,16,17].

Composite 1 wt% loads	VGCF or MWNT parameters		Composite tensile properties	
	Diameter (nm)	Aspect ratio (l/d)	Strength (MPa)	Modulus (MPa)
PS + VGCF	> 200	< 100	~ 1	1190
PS + MWNT	30	> 1000	16	1690

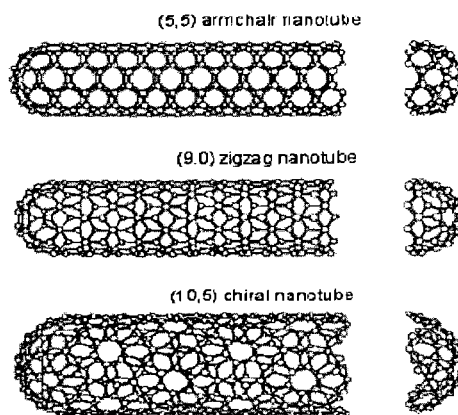
Table 1.2 Mechanical performance of the multi-walled carbon nanotubes (MWNTs) and vapor-grown carbon fibers (VGCF) as reinforcements for polystyrene (PS) composites [19].

Direct-Drive Targets	OMEGA Laser System (U of Rochester)	National Ignition Facility (NIF)
Capsule Diameter (μm)	~ 880	~ 3500
Capsule Wall Thickness (μm)	3-5	< 5
DT Layer Thickness (μm)	100	350

Table 1.3 Designs of Inertial Confinement Fusion (ICF) targets for various laser facilities [21,22].

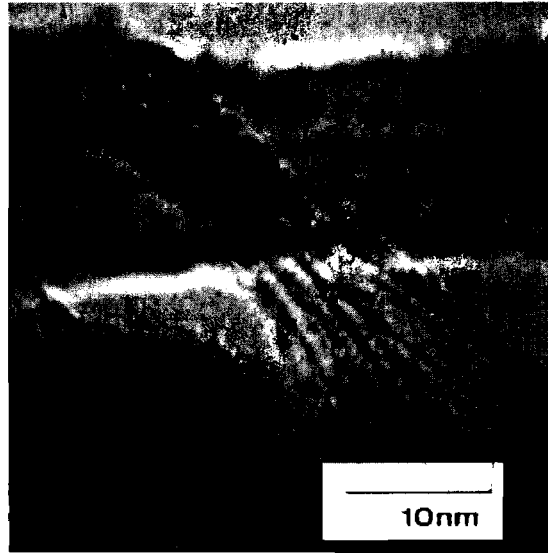


(a)

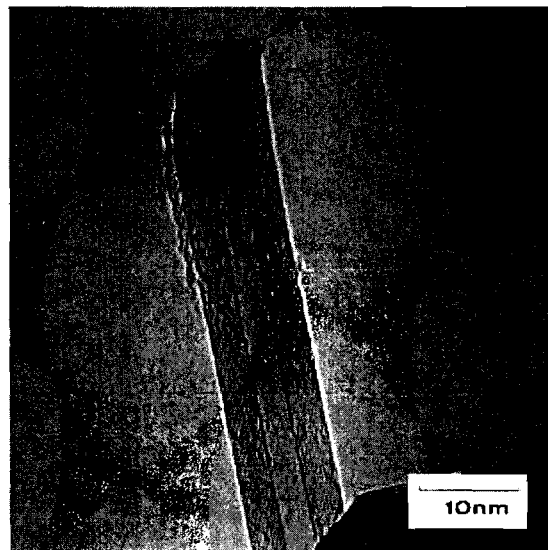


(b)

Figure 1.1 (a) A graphene sheet made of carbon atoms placed at the corners of hexagons forming the lattice with chiral vector, $C_h = na_1 + ma_2$ (a_1 and a_2 are the unit vectors) denoting the rolling direction of the sheet to make (b) a $(5,5)$ armchair nanotube, a $(9,0)$ zigzag nanotube, and a $(10,5)$ chiral nanotube [14].



(a)



(b)

Figure 1.2 TEM images of typical (a) SWNTs, and (b) MWNTs [1,14].

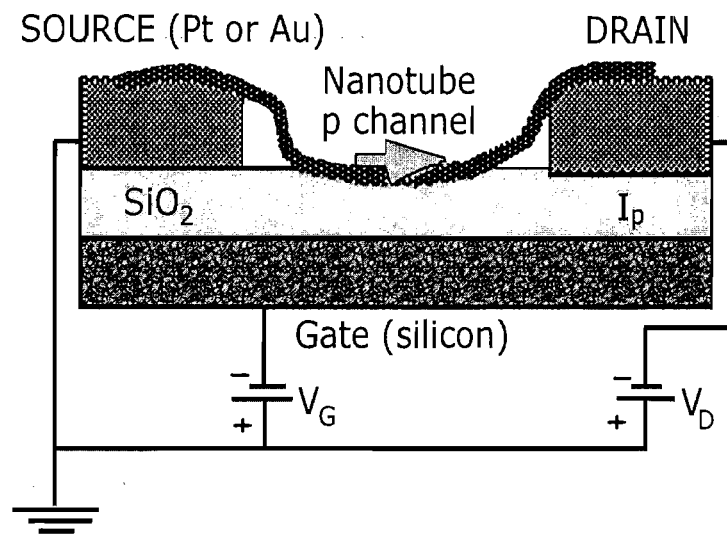


Figure 1.3 Schematic of the carbon nanotubes-based field effect transistor [9,10].

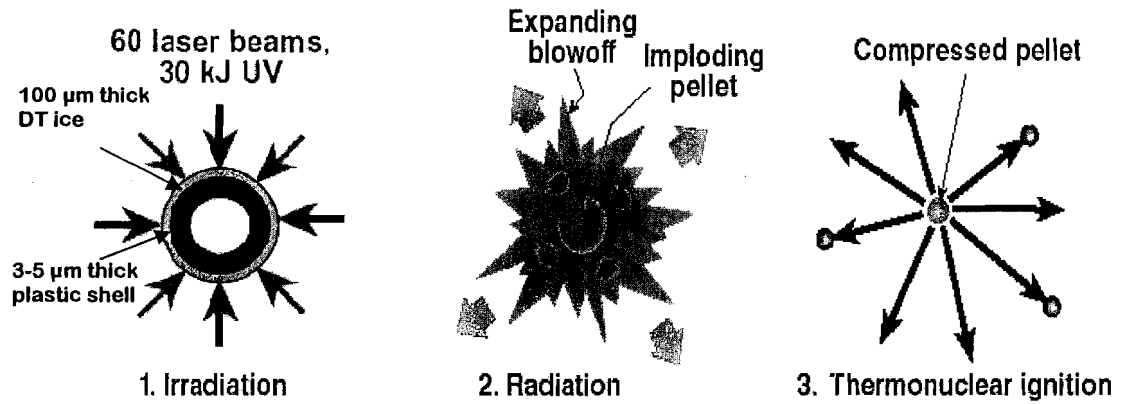


Figure 1.4 Schematics of the Inertial Confinement Fusion (ICF) process [20].

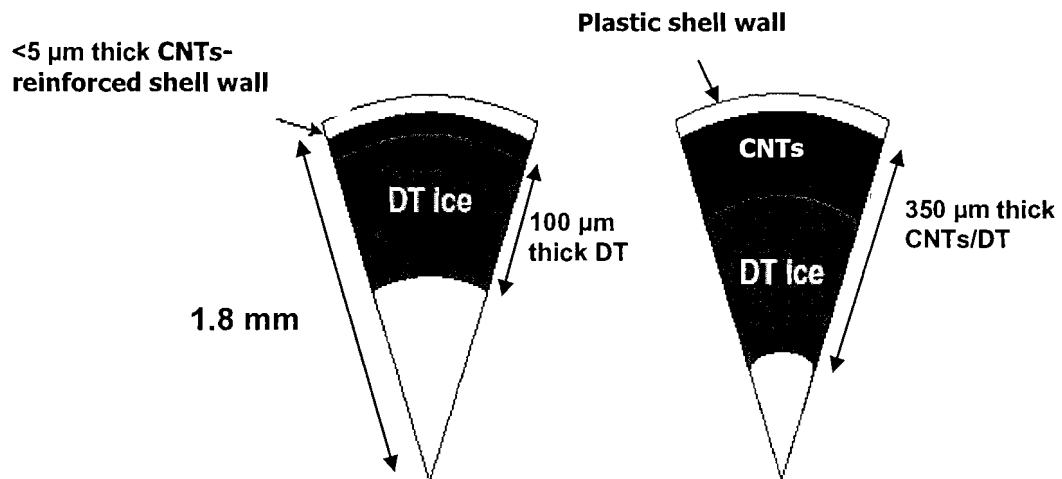


Figure 1.5 Schematics of the typical targets with (a) nanotubes-reinforced shell walls and (b) nanotubes-reinforced DT layers inside the walls.

Chapter 2. Fabrication of Carbon Nanotubes by Microwave

Plasma Chemical Vapor Deposition

2.1 Introduction

2.1.1 Synthesis Methods of Carbon Nanotubes

For the synthesis of high yield and good quality carbon nanotubes, many methods were invented and developed. A summary of some standard nanotubes fabrication techniques is given in Table 2.1. The earliest approach to produce nanotubes was an arc-discharge process [27] as pioneered by Iijima [1]. This was shortly followed by a laser ablation technique developed by Smalley at Rice University [28]. Chemical vapor deposition (CVD) has become a common technique to grow CNTs in the last decade [29-34], with the interest of capable to be scaled for industrial production. Regardless of the applications and growth approach, the ability to control the properties of the nanotubes is critical to realize the promise of carbon nanotubes.

The arc-discharge process involves the use of two graphite electrodes under a gas atmosphere (such as argon or helium) and a voltage is applied until a stable arc is achieved [1,27,35]. This produces SWNTs in mixture of MWNTs and soot. To

synthesize pure SWNTs, an arc discharge with a cathode containing metal catalysts (such as cobalt, iron or nickel) mixed with graphite powder results in a deposit containing SWNTs [28]. The yield has been significantly increased by optimizing the catalyst mixture and the deposition condition.

In the laser ablation method, a target consisting of a mixture of graphite and a metal catalyst (such as cobalt or nickel) is placed in a horizontal quartz tube enclosed in a furnace and under a flow of inert gas at controlled pressure [1]. Laser pulses enter the tube and strike the target to vaporize graphite and nucleate CNTs through the reactor. The nanotubes are deposited on the cooler walls downstream from the furnace. Despite the high temperature (~ 1200 °C) of the furnace, this method has still become an important technique due to the high yield of CNTs ($\sim 70\%$).

Growth of CNTs using thermal chemical vapor deposition (CVD) is an alternative to the arc-discharge and laser ablation methods. It relies on thermal generation of active radicals from the hydrocarbon gas over transition metals to grow CNTs on a substrate, where temperature is normally about 800-1500 °C. Usually, a catalyst is necessary to promote the growth from some form of hydrocarbon feedstock (CH_4 , C_2H_2 , C_2H_4 ...) [36]. It was also reported the yield and average diameter of CNTs could be varied by controlling the process parameters [37].

